Clay Minerals (2026), **61**, 69–81
doi:10.1180/clm.2026.10027

Article

Transforming environmental waste into valuable resources: characterization of clayey sludge from aggregate quarries for sustainable traditional ceramics

Safaa Zahir[1], Lahcen Daoudi[1], Meriam El Ouahabi[2] and Nathalie Fagel[2]

[1]Georesources, Geoenvironment and Civil Engineering Laboratory (L3G), Faculty of Science and Technology, Cadi Ayyad University, Marrakech, Morocco and [2]Laboratory of Clay, Geochemistry and Sedimentary Environment (AGEs), Department of Geology, University of Liege, Belgium

Abstract

The clayey sludge resulting from aggregate washing in quarries of the Marrakech region generates significant environmental impacts and adds an economic burden to the industry. This study aims to characterize these clayey sludges in order to explore their potential for ceramic applications. Fifteen samples were collected from various quarries along the major waterways of the Marrakech region. The physical properties of the clayey materials were analysed according to particle-size distribution and plasticity limits. The mineralogical composition was determined using X-ray diffraction and Fourier-transform infrared spectroscopy. The chemical composition was determined using X-ray fluorescence spectroscopy. The carbonate and volatile contents were determined by calcimetry and loss on ignition at 500°C and 950°C, respectively. SiO_2 and Al_2O_3 are main constituents, while quartz, feldspars and clay minerals are the main phases, along with minor calcite and hematite. Illite is the dominant clay mineral, followed by kaolinite and chlorite. The clayey material exhibits low to medium plasticity and variable particle-size distributions. The chemical composition of these sludges confirms their potential for red ceramic applications. However, their low plasticity, variable particle-size distribution and mineralogical composition, characterized by a low clay mineral content, limit their direct applicability. To improve their suitability for ceramic production, adding clay-rich tempers is essential to enhancing their mineralogical composition, granulometry and plasticity. Furthermore, the results provide a valuable guide for selecting local materials for Marrakech pottery and can serve as a model for other regions.

Keywords: Green ceramic; industrial waste; pottery; recycling; valorization

(Received 3 September 2025; revised 15 February 2026; accepted 15 February 2026; Accepted Manuscript online: 25 March 2026; Associate Editor: Michele Dondi)

Industrial sludges are waste byproducts generated during the transformation of raw materials into finished products through industrial processes. According to the United States Environmental Protection Agency (EPA), sludges can be generated from several industrial activities, mainly paper production (Vashistha *et al.*, 2019), chemical manufacturing (Kologrieva *et al.*, 2022; Magalhães *et al.*, 2024), wastewater treatment (Martínez-García *et al.*, 2012), energy production (Castellanos *et al.*, 2024), metallurgy and mining (Luo *et al.*, 2018; Fatah *et al.*, 2021; El Aallaoui *et al.*, 2025) and the ceramic industry (Avram *et al.*, 2024a). Managing these waste materials is a significant challenge due to their large volumes and the need for extensive landfill areas.

In the Marrakech region (central Morocco), clayey sludges are considered to be another type of harmful waste. They are being disposed of in increasing tonnages, and they result from the washing of aggregates derived from the crushing of alluvial deposits in riverbeds. The rapid population growth in this area has driven urban expansion, requiring the construction of new housing, infrastructure and services. These demographic dynamics significantly increase the demand for construction materials, thereby intensifying the exploitation of natural resources, particularly in aggregate quarries. This amplification generates an accumulation of washing sludge, posing a major environmental challenge due to its complex management and impact on surrounding ecosystems (Loutou *et al.*, 2018). These sludges are often discharged into sedimentation basins. This is a low-cost disposal method widely adopted by the aggregate industries, but it is not a sustainable management solution. Clayey sludges can cause significant ecological disruption, including the accumulation and dispersion of fine solid particles into the air, water and soil (Maletsika *et al.*, 2015; Zia-Khan *et al.*, 2015; Zajec *et al.*, 2016). Therefore, developing a technologically and economically viable recycling solution could provide commercial opportunities while simultaneously reducing the environmental footprint of the aggregate industries.

Corresponding author: safaa zahir; Email: safaa.zohir@gmail.com

Paper submitted for the special issue devoted to the ICC

Cite this article: Zahir S, Daoudi L, El Ouahabi M and Fagel N (2026) Transforming environmental waste into valuable resources: characterization of clayey sludge from aggregate quarries for sustainable traditional ceramics. *Clay Minerals* **61**, 69–81. https://doi.org/10.1180/clm.2026.10027

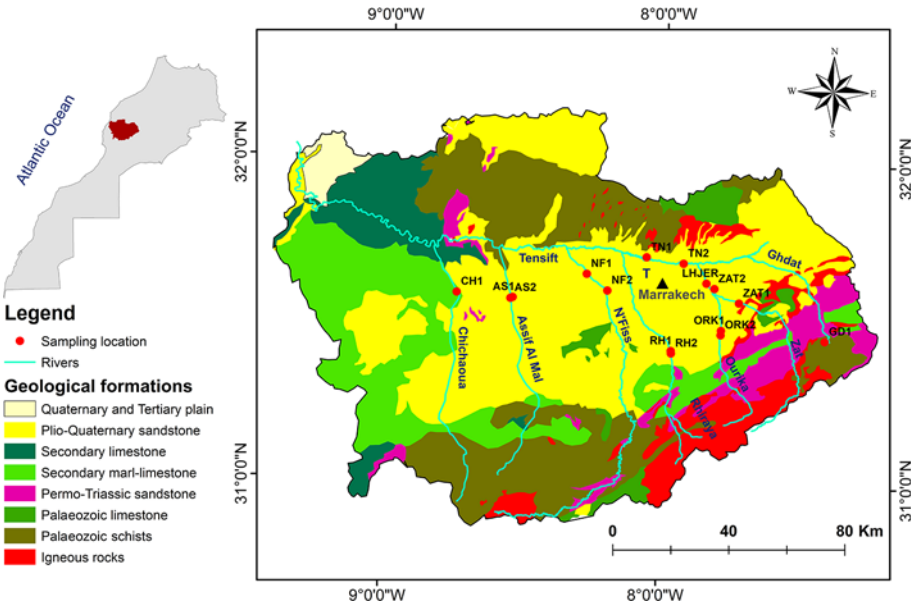

Figure 1. Geological map of the Tensift watershed and locations of the samples studied.

The reuse of industrial sludge in ceramic manufacturing, either as a primary raw material or as a substitute for conventional materials, has been demonstrated by several studies as an effective solution for contaminant confinement, reducing sludge amounts, landfill storage needs and costs (González-Corrochano *et al.*, 2009; Galetakis *et al.*, 2012). For instance, in Poland, waste generated from dolomite aggregate washing has been successfully used in ceramic pastes without prior treatment (Kłosek-Wawrzyn *et al.*, 2019), and in Egypt, incorporating 10–40 wt.% granite sludge into ceramics improved material density and reduced porosity (Sadek *et al.*, 2021). Similarly, in Spain, the addition of 5% wastewater sludge to clay raw materials improved clay brick properties (Martínez-García *et al.*, 2012). In India, lime sludge can replace up to 20% of the materials used in brick manufacturing, reducing energy consumption, as the sintering lime sludge-based bricks occurs at a lower temperature (Vashistha *et al.*, 2019). In Romania, sludge from wastewater generated during ceramic tile processing can be valorized as a raw material for ecological building materials, and moderate thermal consolidation allows the production of bricks of good to high quality and a low carbon footprint (Avram *et al.*, 2025).

Quarry mining is a crucial sector supporting the economy of Morocco and its social development, particularly in terms of infrastructure and housing (Ministère de l'Equipement du Transport et de la Logistique, 2016). A national inventory conducted in 2012 identified 1885 quarries across Morocco, with more than 238 quarries located in the Marrakech region alone (Ministère de l'Équipement et du Transport, 2012; Haut Commissariat au Plan, 2020).

The Marrakech region is renowned for its centuries-old ceramic industry, with hundreds of small artisanal workshops operating around the city. The raw clay material used by artisan potters is sourced from local deposits. However, due to their poor quality, artisans often import raw materials from other Moroccan regions, such as Fez, Safi and Sale, to improve their properties through blending (Daoudi *et al.*, 2014; El Boudour El Idrissi *et al.*, 2016).

Although various types of industrial sludge have been extensively documented in the literature, sludge from the aggregate industry remains underexplored. This study aims to address this research gap by characterizing sludges from different quarries in the Marrakech region. It aligns with a broader strategy aiming to improve the recycling of clayey sludge generated during aggregate washing. The main objective is to assess the extent to which this sludge can be used as a raw material for the production of ceramic bodies, which could potentially reduce production costs. Additionally, this approach could also have a positive environmental impact by preventing sludge discharge into nature and mitigating the associated environmental issues.

Study area

The study area is part of the Tensift watershed, located in central Morocco, covering an area of 20,450 km^2. It is characterized by an arid to semi-arid climate, moderated by complex orographic features (Hajhouji, 2018). From a geomorphological perspective, the basin comprises an alluvial plain, which accounts for 70% of the total basin area, bordered to the north by the Jebilet mountain range (10%), with altitudes up to 1000 m, and to the south by the High Atlas mountain range (20%), with a maximum elevation of 4170 m (Haida *et al.*, 1996). The plain is traversed by the Tensift River, flowing from east to west, and its main tributaries mainly located on the left bank (i.e. Chichaoua, Assif Al Mal, N'Fiss, Rhiraya, Ourika, Zat and Ghdat). The aggregate quarries studied are located along these rivers (Fig. 1).

Geologically (Fig. 1), the southern part of the basin, which belongs to the High Atlas mountain range, is primarily composed of Palaeozoic magmatic and metamorphic rocks (Michard *et al.*, 2008). Its northern part is characterized by Mesozoic to Quaternary sedimentary formations, including limestones, dolomites, marls, clays and sandstones (Haida *et al.*, 1996).

Materials and methods

Materials

To characterize the clayey sludges discharged by aggregate quarries in the Marrakech region, 15 samples were collected from the largest quarries along the main watercourses of the Tensift Basin (Fig. 2).

Figure 2. (a) Direct discharge of clayey sludge. (b & c) Clay extracted from sedimentation basins and then stored.

The sampling strategy consisted of collecting the clayey sludges derived from different watercourses and identifying potential variations in composition within the same tributary. Accordingly, one or more samples were collected from each stream.

The sample were labelled based on the name of the watercourse where the quarry is located: two samples were collected from Tensift (TN1, TN2), one sample from Ghdat (GD1), two samples from Zat (ZAT1, ZAT2), two samples from Ourika (ORK1, ORK2), one sample from Lhjer (LHJER1), two samples from Rhiraya (RH1, RH2), two samples from N'Fiss (NF1, NF2), two samples from Assif Al Mal (AS1, AS2) and one sample from Chichaoua (CH1). For each quarry, a single representative raw sample was collected. Sampling was conducted directly from the waste storage areas located within or near the quarries, with the assistance of local workers. All samples exhibited a homogeneous reddish-brown colouration and a predominantly silty texture. Over 20 kg of material was collected for each sample. To ensure representative sampling, the sludges from each quarry were mixed and divided using the quartering method. The sludges were used as received, without any calcination or chemical modification.

Methods

The samples were pre-dried at 45°C for 48 h before analysis. The particle-size distribution of the samples was determined using a Horiba LA-300 laser diffraction analyser (Cadi Ayyad University). The sand fraction (>63 μm) was first separated *via* wet sieving. For the silty-clay fraction (<63 μm), ~1 g of the sample was placed in a container with 100 mL of demineralized water for 24 h. The sample was then stirred on a magnetic plate to break up aggregates before analysis. Three measurements were performed for each sample to ensure reproducibility.

The mineralogical composition was determined by X-ray diffraction (XRD) on both powdered bulk sediment and the <2 μm fraction, using a Bruker D8 Advance powder diffractometer. The diffractometer operates with Cu-$K\alpha$ radiation in which the $K\alpha_1$ and $K\alpha_2$ components remain unseparated, yielding an effective composite wavelength of $\lambda = 1.5418$ Å. Scans were performed with a step size of 0.02° and a time per step of 0.6 s, corresponding to a scanning rate of ~0.02° min^{-1}. This diffractometer was connected to a high-voltage generator (40 kV, 30 mA, 1200 W) and coupled to *EVA*® Bruker software (University of Liège, Belgium). The clay fraction (<2 μm) was obtained from 1–2 g of raw sample previously sieved at 63 μm. The carbonates were removed with 0.1 M HCl under agitation and then washed several times under centrifugation to obtain a stable suspension. The <2 μm fraction was separated by gravity sedimentation according to Stokes' law. The first centimetre of the suspension was collected with a pipette, placed on a glass slide and air-dried overnight at room temperature (Moore & Reynolds, 1997). Orientated aggregates were then analysed using XRD, and for each sample three XRD traces were recorded after successive treatments: air-dried, ethylene glycol (EG)-solvated for 24 h and heated at 500°C for 4 h. A semi-quantitative estimation of the bulk mineralogy was conducted according to Cook *et al.* (1975). Peak assignment was carried out using the *HighScore Plus*® Panalytical software coupled to the PDF-2 database of the International Centre for Diffraction Data (ICDD). The reflection at 19.88° was used to estimate the total abundance of clay minerals (Boski *et al.*, 1998). The main clay minerals were semi-quantified according to the Holtzapffel (1985) method, which applies corrective factors to the intensities of each peak in EG runs.

Scanning electron microscopy (SEM) was employed as a complementary technique to characterize the structure and morphology of the samples. Microstructural analyses were conducted at

Table 1. Mineralogical composition of the bulk and clay fractions (wt.%).

	Bulk fraction										Clay fraction					
Sample	Qz	Kfs	Pl	Cal	Dol	Hem	Amp	Ilt-Mca	Ant	Tc	Kln	Chl	Ilt	Sme	Vrm	Chl-Sme ML
AS1	31	9	29	2	3	1	1	10	1	13	0	1	11	0	1	0
AS2	36	9	23	2	4	1	1	12	2	11	0	0	8	0	2	0
CH1	43	0	7	15	8	5	0	4	1	16	1	0	10	4	0	0
GD1	53	9	23	1	1	2	4	2	1	6	0	0	5	0	1	0
LHJER1	65	4	21	0	0	2	1	1	0	6	0	0	3	0	2	0
NF1	41	6	18	6	3	1	0	6	1	19	0	0	15	3	1	0
NF2	36	8	28	2	1	5	0	2	0	19	2	0	12	3	1	1
ORK1	42	8	34	1	1	1	2	2	0	10	1	0	8	0	2	0
ORK2	43	11	15	1	1	2	2	3	1	21	2	1	9	0	9	0
RH1	43	11	15	1	1	2	2	3	1	21	1	0	14	3	0	1
RH2	42	8	16	3	6	3	0	5	0	17	1	0	11	3	0	2
TN1	43	4	11	6	1	2	0	6	1	24	3	0	14	6	1	0
TN2	43	24	10	2	1	1	1	3	0	15	1	0	9	3	0	1
ZAT1	61	8	17	1	1	1	1	2	1	8	1	0	6	0	1	0
ZAT2	50	19	20	1	1	1	1	1	0	6	1	0	4	0	1	0

Amp = amphibole; Ant = anatase; Cal = calcite; Chl = chlorite; Dol = dolomite; Hem = hematite; Ilt = illite; Ilt-Mca = illite-mica; Kln = kaolinite; Kfs = K-feldspar; ML = mixed layers; Pl = plagioclase; Qz = quartz; Sme = smectite; Tc = total clay; Vrm = vermiculite.

Université Le Havre Normandie (LOMC) using a ZEISS Gemini Sigma 360 VP (Carl Zeiss, Germany) operating in a high-vacuum mode with an accelerating voltage of 20 kV. Observations were performed using SE1 and InLens detectors. All samples were gold-coated using an EmScope sputtering device.

The Fourier-transform infrared (FTIR) spectroscopy analysis was performed using a Bruker Vertex 70 spectrophotometer in transmission mode (Cadi Ayyad University). Pellets were prepared by combining 1 mg of sample powder with 99 mg of KBr. The measurements were performed over a spectral range of 400–4000 cm^{-1} by averaging 32 scans at a resolution of 4 cm^{-1}. This analysis allows for the identification of the chemical bonds present in the studied materials and confirms the crystalline phases revealed by XRD.

The chemical analysis of the major elements was carried out *via* X-ray fluorescence (XRF) spectroscopy using a Panalytical Axios spectrometer equipped with an Rh tube and argon/methane gas (Cadi Ayyad University). Before XRF analysis, the samples were heated at 550°C for 4 h, followed by 950°C for 2 h in a furnace to determine the loss on ignition (LOI; Heiri *et al.*, 2001). The carbonate content was determined using Bernard's calcimetry technique.

The plasticity of the samples was determined using Atterberg limits: liquid limit (LL) and plastic limit (PL). The plasticity index (PI) was calculated as the difference between the LL and PL values for the analysed samples (Cadi Ayyad University). The LL tests were performed using a penetration cone, following the NF P94-051 and NF P94-052 standards (AFNOR, 1993, 1995).

Results and discussion

Mineralogical composition

The mineralogical composition varies considerably from one site to another (Table 1). The XRD traces are shown in Fig. S1. The identified mineral phases include clay minerals, quartz (PDF-2 00-033-1161), K-feldspar (PDF-2 01-089-8572), plagioclase (PDF-2 00-002-0537), carbonates such as calcite (PDF-2 00-002-0623) and dolomite (PDF-2 00-011-0078), hematite (PDF-2 00-001-1053), mica-illite (PDF-2 00-001-1098) and traces of amphibole (PDF-2 01-089-7282) and anatase (PDF-2 01-071-1168).

Quartz is the dominant mineral in all samples, with contents ranging from 31 to 65 wt.%, and with the highest amounts observed in samples from the Lhjer, Zat and Ghdat riverbeds. The abundance of quartz is attributed to the upstream geological formations, composed of Permo-Triassic continental red silty sandstone deposits, and to the occurrence of acidic leucocratic magmatic rocks in this part of the basin (Fig. 1). The Lhjer River sample (LHJER1) stands out for having the highest quartz content due to its supply from the Zat and Ourika rivers, which intensify the siliceous input. The high quartz content of the samples underscores their resistance to mechanical weathering during transport. In contrast, samples from the Assif Al Mal (AS1, AS2) exhibit the lowest quartz content (<35%), attributed to the predominance of sedimentary formations in the south-western part of the basin. These regions include Permian and Quaternary formations, mainly composed of shales and carbonates. Furthermore, this also explains the higher mica-illite content of the Assif Al Mal samples: 10 wt.% in AS1 and 12 wt.% in AS2.

The samples are also rich in plagioclase (7–34 wt.%), and K-feldspar is present in all samples except CH1, with amounts varying between 4 and 24 wt.%. The distribution of K-feldspar is related to the nature of the upstream outcrops along the corresponding watercourses.

Overall, the calcite content does not exceed 6 wt.% in these wastes, except in the CH1 sample taken from the Oued Chichaoua, which contains 15 wt.%. Similarly, the dolomite content is generally lower than 6 wt.%, with a maximum of 8 wt.% in sample CH1. Most samples displayed a total carbonate content of less than 10 wt.%, except for sample CH1 (20 wt.%). This higher carbonate content is linked to its location in the western part of the basin, an area with abundant secondary marl-limestone outcrops. All samples contain <5 wt.% hematite, and amphibole and anatase are accessory phases, with contents below 2 wt.%.

The XRD traces of the clay fractions depict distinct mineralogical compositions. The samples contain illite, kaolinite, chlorite, smectite, vermiculite and ordered mixed-layer chlorite-smectite. Kaolinite was identified by the reflections at 12.4°2θ and 24.9°2θ,

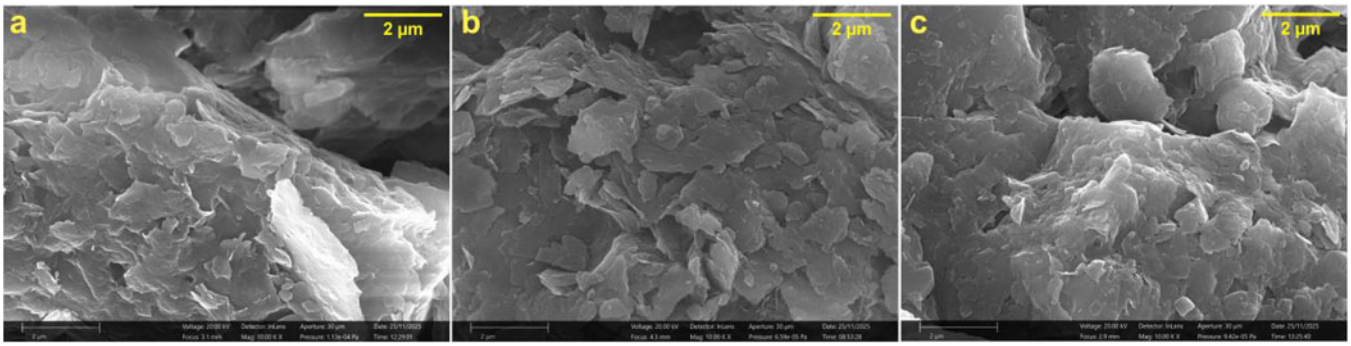

Figure 3. SEM images of the samples: (a) NF2, (b) TN2 and (c) ZAT1.

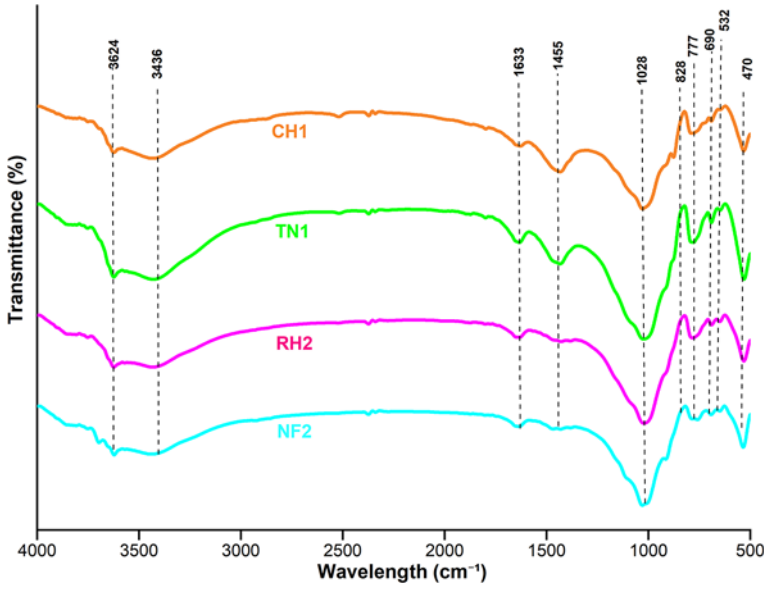

Figure 4. FTIR spectra of the studied samples.

which remain after EG solvation but disappear after heating at 500°C for 4 h. Illite was recognized by reflections at 8.8°2θ, 17.7°2θ and 27°2θ, which were not affected by glycolation and heating treatments. Smectite was identified by the peak at 5.9°2θ under ambient conditions, which shifts to ~5°2θ after EG solvation and collapses to 8.8°2θ upon heating. Chlorite was identified by basal reflections at 6.3°2θ, 12.7°2θ, 18.9°2θ and 25.5°2θ, which were not affected by glycolation and heating (Holtzapffel, 1985). Vermiculite also shows a reflection at 6.3°2θ, which decreases and collapses to 8.8°2θ upon heating. These peaks may be attributed to chlorite that has undergone alteration into vermiculite (April *et al.*, 1986; Tomanec *et al.*, 1997). Ordered mixed-layer chlorite-smectite was identified by a first-order superstructure peak at 3.2°2θ under ambient conditions, expanding to 2.9°2θ after EG solvation and contracting to 3.7°2θ after heating (Thorez, 1976).

The total clay content ranges from 6 to 24 wt.%, with the most clay-rich samples originating from quarries located along watercourses frequently affected by flooding (i.e. Ourika, Rhiraya and Tensift), which are the main sources of the clay deposits used for aggregate production (Saidi *et al.*, 2003; El Khalki *et al.*, 2020). Illite is the most abundant clay mineral phase in all samples, accounting for 3–15 wt.% of the total composition. Illite displays narrow diffraction peaks, indicating a high crystal order. This suggests that the illite originates from Palaeozoic schists of the High Atlas mountain range (Gourfi *et al.*, 2020). The most illite-rich samples correspond to watercourses draining basins dominated by metamorphic shale outcrops (N'Fiss, Rhiraya and Assif Al Mal). Kaolinite and vermiculite are ubiquitous but present at low contents (<3 wt.%), except for the sample from the Ourika River (ORK2), for which the vermiculite content reaches 9 wt.%. Chlorite and ordered mixed-layer chlorite-smectite clays are detected in trace amounts (<2 wt.%). Smectite is absent in most wastes, except for those of Tensift (TN1 and TN2), Chichaoua (CH1), Rhiraya (RH1 and RH2) and N'Fiss (NF1 and NF2), where it ranges from 3 to 6 wt.%. The occurrence of smectite in these samples is linked to smectite-rich Meso-Cenozoic sedimentary formations (Daoudi *et al.*, 2014, 2015; Knidiri *et al.*, 2014; Gourfi *et al.*, 2020).

SEM images of the samples (Fig. 3) reveal that the fine fraction is dominated by stacked lamellar particles characteristic of illite. The particles exhibit irregular edges and a typical 2:1 phyllosilicate texture. No fibrous or tubular morphologies were observed. These observations confirm the mineralogical composition determined by XRD, with illite dominating the clay fraction.

The FTIR spectra (Fig. 4) display characteristic absorption bands of clay minerals, quartz, feldspars and carbonates, consistent with the XRD results. Detailed band assignments are summarized in Table 2. The absorption bands at 3624 and 3436 cm^{-1} are attributed to the O–H stretching vibrations of structural

Table 2. FTIR absorption band assignment.

Absorption band (cm^{-1})	Assignment	Compound	Reference
3624	O–H stretching	Clay minerals	Saikia *et al.* (2003)
3436	O–H stretching of adsorbed water	Clay minerals (adsorbed water)	Madejova (2003)
1633	H–O–H bending	Adsorbed water	Mercantili *et al.* (2013)
1455	CO_3 bending (carbonate)	Calcite, dolomite	Veerasingam & Venkatachalapathy (2014)
1028	Si–O stretching	Quartz, feldspars, clay minerals	Saikia *et al.* (2003), Maston *et al.* (2025)
828	Al–O stretching	Clay minerals	Tarte (1967), Avram *et al.* (2025b)
777	Si–O–Si bending	Quartz	Unuabonah *et al.* (2013)
690	Si–O stretching	Quartz	Saikia *et al.* (2003)
532	Al–O–Si deformation	Clay minerals	Saikia *et al.* (2003)
470	Si–O bending	Quartz	Saikia *et al.* (2003)

hydroxyl groups in clay minerals and to adsorbed water, respectively (Madejova, 2003; Saikia *et al.*, 2003). The band at 1633 cm^{-1} corresponds to the H–O–H bending vibration of molecular water (Mercantili *et al.*, 2013), indicating surface and interlayer water associated with the phyllosilicates. The band at 1455 cm^{-1} is characteristic of the carbonate group (CO_3) and is assigned to calcite and dolomite (Veerasingam & Venkatachalapathy, 2014). This band is more intense in the CH1 and TN1 samples, reflecting their greater carbonate contents, which is in agreement with the XRD data.

The strong absorption band at 1028 cm^{-1} corresponds to the Si–O stretching vibration of silicates, namely quartz, feldspars and clay minerals (Saikia *et al.*, 2003; Maston *et al.*, 2025). Quartz is further confirmed by the bands at 777 and 690 cm^{-1}, assigned to Si–O–Si bending and Si–O stretching, respectively (Saikia *et al.*, 2003; Unuabonah *et al.*, 2013). The band at 470 cm^{-1} is also related to the Si–O bending vibration (Saikia *et al.*, 2003). The absorption at 828 cm^{-1}, assigned to Al–O stretching, together with the band at 532 cm^{-1} attributed to Al–O–Si deformation, confirms the presence and structural organization of phyllosilicate clay minerals and feldspars (Tarte, 1967; Saikia *et al.*, 2003; Avram *et al.*, 2025b).

The mineralogical composition of the samples, dominated by quartz, feldspars and illite, presents both advantages and potential limitations that should be considered for ceramics manufacturing. Quartz and feldspars contribute to the formation of a glassy phase during firing, with feldspars acting as fluxes to lower the melting temperature and promote mullite crystallization, and partially unmelted quartz ensures a rigid structure and improves the mechanical properties of ceramics (Lee & Yeh, 2008; Baccour *et al.*, 2009; Maalla *et al.*, 2021). However, a high quartz content (>50 wt.%) may cause thermal expansion and cracking, and a high carbonate content (>10 wt.%; e.g. sample CH1) may inhibit mullite formation and may induce bloating or whitening of the ceramic material (Dondi *et al.*, 2014; El Ouahabi *et al.* 2015). Therefore, for samples rich in quartz and carbonates, it may be necessary to consider formulations by blending them with other clays to render their mineralogy more suitable for ceramic production.

Previous work has demonstrated the favourable properties of illitic clays for ceramic applications (Bennour *et al.*, 2015). Illite plays an essential role in traditional ceramics as the main components used in the production of plates, pots, tiles and bricks (Ferrari & Gualtieri, 2006). It improves sintering by increasing the glassy phase, reducing water absorption and lowering the melting temperature (Garzón *et al.*, 2010). However, an excessive illite content may cause linear shrinkage and inhibit mullite, cristobalite and quartz formation in the fired products (Carretero *et al.*, 2002). In this study, the moderate illite content prevents such adverse effects. Smectites are present in only a few samples, with concentrations below 5 wt.%. This low concentration is beneficial as it prevents cracking related to the swelling and shrinkage associated with higher smectite levels (Aydinalp, 2010).

The ternary diagram by Strazzera *et al.* (1997), based on the proportions of clay minerals, quartz, feldspars and carbonates, highlights the relationship between the mineralogical composition of the samples and their potential for ceramic applications (Fig. 5). It is evident that only one sample from Oued Tensift (TN1) is projected within the zone corresponding to structural clay ceramics, demonstrating its suitability for ceramic production without the need for any additives. In contrast, the remaining samples fall outside this applicability zone, mainly due to their low clay mineral content. To make these raw materials compatible with ceramic production, the addition of clay-rich minerals would be essential to improve their mineralogical composition.

Chemical composition

Table 3 lists the chemical composition of the studied samples, showing that SiO_2 is the most abundant oxide (56–77 wt.%), followed by Al_2O_3 (9–14 wt.%) and Fe_2O_3 (4–7 wt.%). Most samples exhibit low CaO contents (<5 wt.%), except for CH1 (12 wt.%), consistent with the XRD and Bernard's calcimetry results. K_2O (2–3 wt.%) and MgO (2–4 wt.%) are also abundant, whereas Na_2O (0–3 wt.%) and TiO_2 (0.6–1 wt.%) are relatively low in content, and MnO and P_2O_5 are present only in trace amounts. The concentrations of CaO, MgO and Fe_2O_3 confirm the presence of calcite, dolomite and hematite, respectively, as detected by the XRD analysis. The LOI values at 950°C range from 1 to 10 wt.%. These variations are attributed to the presence of organic matter, the dehydroxylation of hydrated minerals and the decomposition of carbonates. The highest LOI values (>9 wt.%) are observed in the carbonate-rich samples (TN1 and CH1), whereas the lowest LOI values (<6 wt.%) are found in samples with a low carbonate content (<2 wt.%).

The colour of ceramics is primarily controlled by the Fe_2O_3 content and the firing temperature (Kreimeyer, 1987), as well as by the Fe_2O_3/CaO ratio (Fiori *et al.*, 1989). When Fe_2O_3 exceeds 5 wt.%, ceramics exhibit a red colour after firing, whereas those containing 1–5 wt.% Fe_2O_3 become beige, and those with an Fe_2O_3 content below 1 wt.% produce whitish-coloured ceramics (Fiori *et al.*, 1989; Murray, 2007; Baccour *et al.*, 2009). A high CaO content can impart yellowish and pinkish tones to pottery (Dondi *et al.*, 2014). Other oxides, such as MgO, MnO and TiO_2, also impact ceramic colour (Kreimeyer, 1987). With an average Fe_2O_3 content of 5.33 wt.%, the samples studied would probably have a red colour after firing. The total alkali and alkaline earth element contents (K_2O, Na_2O, MgO, CaO) exceed 7 wt.%, indicating sufficient fluxing minerals to enhance ceramic fusion (Miliani & Corbara, 1999).

The chemical data provide insights into the phases formed during firing, although transformations remain complex due to interactions between the structural and chemical properties. The

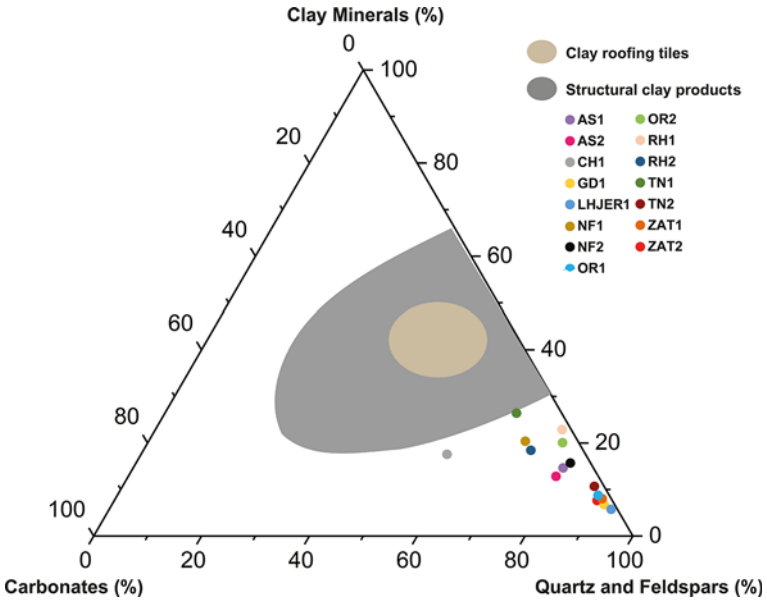

Figure 5. Projection of the studied samples in the ternary diagram modified from Strazzera *et al.* (1997).

Table 3. Chemical compositions (wt.%) of the raw samples.

Sample	SiO_2	Al_2O_3	Fe_2O_3	MgO	MnO	CaO	K_2O	Na_2O	TiO_2	P_2O_5	LOI
AS1	61.6	13.5	5.7	3.6	0.3	4.4	2.6	1.1	0.9	0.1	6.2
AS2	64.4	12.6	4.6	2.7	0.1	5.2	1.9	0.6	0.8	0.1	7.1
CH1	56.1	9.6	4.4	3.6	0.1	11.9	2.2	1.3	0.8	0.0	10.1
GD1	75.9	9.1	4.5	2.4	0.1	2.7	1.8	1.1	0.7	0.2	1.4
LHJER1	76.7	8.6	4.6	2.3	0.2	2.2	1.8	0.7	1.0	0.2	1.7
NF1	63.3	11.7	5.0	3.0	0.6	3.9	2.4	2.3	0.9	0.1	6.8
NF2	64.4	14.3	6.7	2.2	0.1	2.0	3.0	0.6	1.0	0.3	5.5
ORK1	73.0	11.5	4.6	2.0	0.1	2.2	2.2	0.2	0.7	0.2	3.5
ORK2	66.5	13.4	5.8	2.8	0.1	1.6	2.7	0.4	0.8	0.2	5.8
RH1	63.9	13.1	6.1	3.0	0.2	2.9	3.4	0.4	0.9	0.2	5.9
RH2	61.5	12.4	5.9	4.3	0.2	2.9	3.1	1.4	0.8	0.1	7.4
TN1	59.2	12.2	6.0	4.2	0.1	4.8	2.8	0.4	0.8	0.1	9.4
TN2	64.2	12.0	5.9	2.7	0.3	3.4	3.0	1.4	0.9	0.2	6.1
ZAT1	74.4	9.4	3.8	3.4	0.1	2.0	2.3	0.5	0.6	0.2	3.5
ZAT2	75.1	9.0	3.9	2.4	0.1	1.9	2.2	2.5	0.7	0.2	2.0

LOI = loss on ignition at 950°C.

studied samples, characterized by low $CaCO_3$ content and high Al_2O_3 content, would favour mullite formation, primarily driven by the Al_2O_3 content (Khalfaoui & Hajjaji, 2009; El Ouahabi *et al.*, 2015; Laita & Bauluz, 2018). However, a higher CaO content inhibits mullite formation (Trindade *et al.*, 2009, 2010; El Ouahabi *et al.*, 2015), yielding gehlenite, diopside and anorthite instead (Trindade *et al.*, 2009, 2010).

Figure 6 illustrates the projection of the chemical analysis data onto a Fiori *et al.* (1989) ternary diagram ((Fe_2O_3 + CaO + MgO)–Al_2O_3–(Na_2O + K_2O)), classifying clay raw materials and industrial ceramic products. All of the studied samples are projected within the red ceramics field (red circle in Fig. 6), as expected for clays with ≥5% Fe_2O_3 (Murray, 2007; Baccour *et al.*, 2009). The chemical composition confirms their suitability for red ceramic applications in the ceramics industry. However, samples with very high SiO_2 (>75 wt.%) and low Al_2O_3 contents (<9 wt.%) are sandy and may not be directly suitable for red ceramic production without further processing or adjustment, as their mechanical behaviour during shaping and firing could be adversely affected.

Physical properties

The studied clayey sludges exhibit a variable particle-size distribution across the samples (Table 4). The clay, silt and sand fractions vary from 8% to 41%, from 10% to 65% and from 0% to 82%, respectively. The silt fraction represents the dominant component, with an average of 45%. The sample from Oued Lhjer (LHJER1) is characterized by the lowest clay content (<10%) and the highest sand content (>80%).

The SEM images (Fig. 7) confirm the particle-size analysis and reveal a clear morphological contrast between the two samples: ZAT1 (Fig. 7a) enriched in clay-sized fractions (45%) and LHJER1 (Fig. 7b) dominated by sandy fractions (88%). ZAT1 mainly consists of very fine particles with irregular shapes, frequently forming small aggregates, typical of clay-sized materials. In contrast, LHJER1 is composed of well-separated, sand-sized grains exhibiting angular to sub-angular morphologies and a wide size range. In both samples, the predominance of angular shapes and irregular particle surfaces reflect the mechanical origins of the sludges, resulting from crushing, screening and washing.

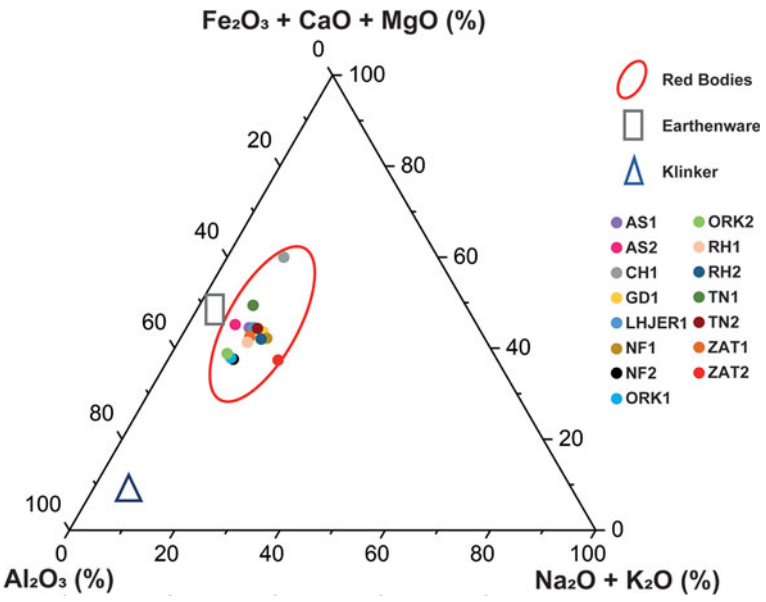

Figure 6. Projection of the chemical compositions of the samples onto a (Fe_2O_3 + CaO + MgO)–Al_2O_3–(Na_2O + K_2O) diagram (modified from Fiori *et al.*, 1989).

Table 4. Physicochemical properties of the analysed samples.

Physical property (%)	AS1	AS2	CH1	GD1	LHJER1	NF1	NF2	ORK1	ORK2	RH1	RH2	TN1	TN2	ZAT1	ZAT2
Particle-size distribution															
Clay <2 µm	20.0	11.8	22.1	12.4	7.9	21.4	16.3	25.4	24.3	14.2	22.4	34.2	24.8	11.3	41.3
2 µm < silt < 63 µm	53.6	55.1	56.7	14.9	9.9	64.7	36.5	33.4	61.4	44.1	54.8	64.8	57.5	19.1	53.1
Sand >63µm	26.4	33.1	21.1	72.7	82.3	13.9	47.3	41.2	14.3	41.7	22.8	1.0	17.7	69.6	5.6
Consistency limits															
LL	29.3	34.6	23.9	27.9	32.4	36.3	26.1	22.5	36.3	39.1	33.2	39.6	31.5	25.4	32.4
PL	22.6	28.1	20.2	22.6	22.6	22.7	21.2	18.5	23.0	25.2	22.7	27.4	21.0	21.5	27.1
PI	6.7	6.5	3.7	5.3	9.8	13.6	4.9	4.0	13.3	13.9	10.5	12.2	10.5	3.9	5.3
LOI (550°C)	2.9	2.0	2.0	1.0	0	3.0	3.0	2.0	4.0	4.0	2.0	4.0	2.9	2.0	1.0
$CaCO_3$ content	2.7	2.2	8.3	0	0	2.0	1.3	0	1.1	4.1	1.3	4.1	1.0	2.2	1.1

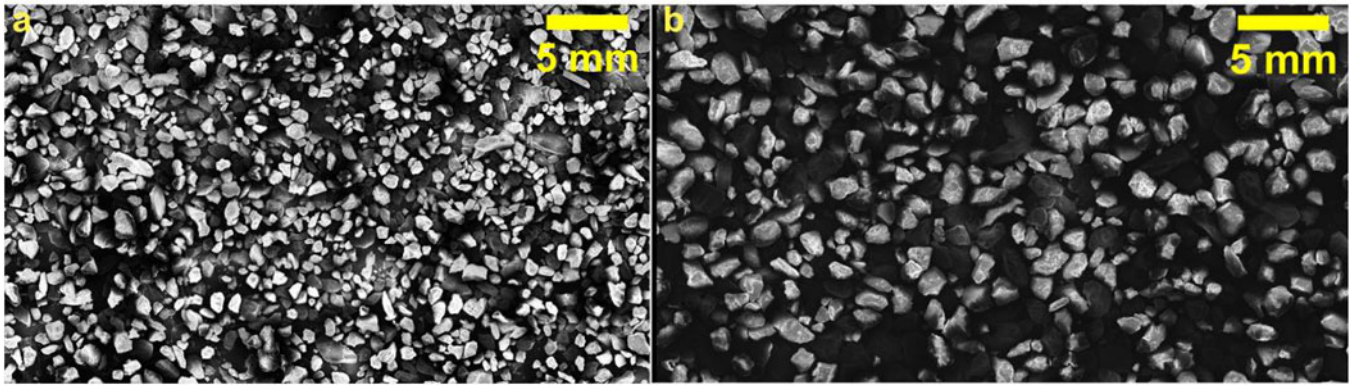

Figure 7. SEM images of the samples: (a) ZAT1 and (b) LHJER1.

The results of the particle-size analysis fit the Shepard ternary diagram (Fig. 8a; Shepard, 1954), highlighting the presence of five textural classes ranging from a silty-clay to sandy texture. Clayey-silt and sandy-silt-clay textures are dominant. The observed granulometric differentiation can be attributed to the nature and the hardness of the parent rocks, which vary between streams, and to the hydrodynamic and sedimentary processes related to transport and deposition, which influence the distribution of these materials within the same watercourse (Gugliotta *et al.*, 2020; Wang *et al.*, 2022).

The particle-size distribution is a key factor in determining the physical properties of a material, including drying shrinkage, mechanical strength, porosity, permeability and clay plasticity (Daoudi *et al.*, 2014; El Boudour El Idrissi *et al.*, 2018;

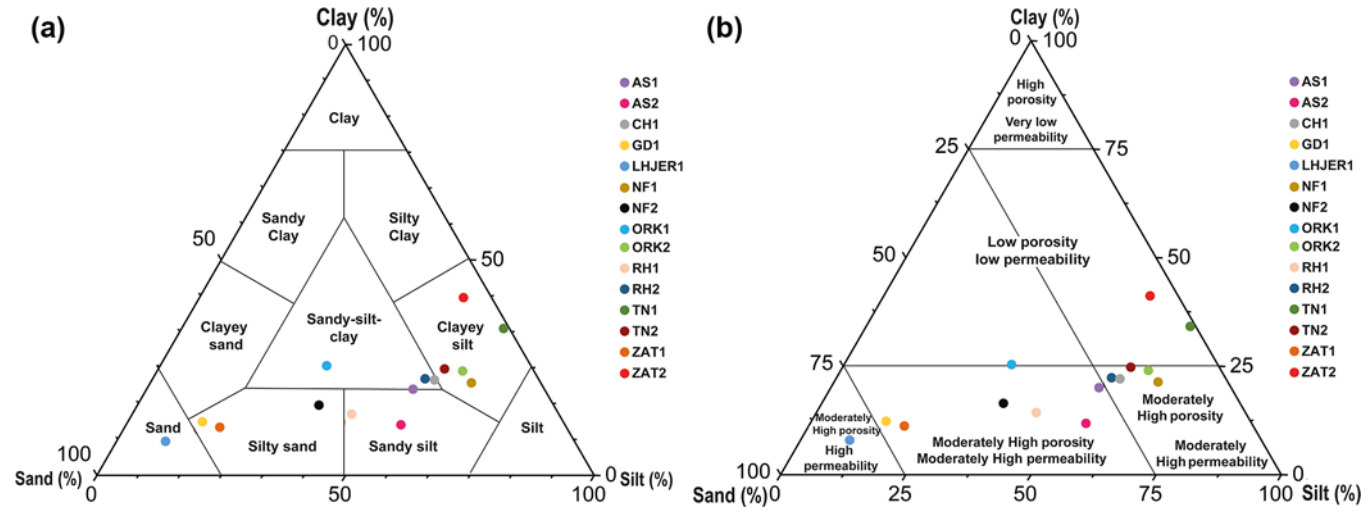

Figure 8. (a) Projection of the analysed samples in the ternary diagram modified from Shepard (1954); (b) textural classification modified from McManus (1988).

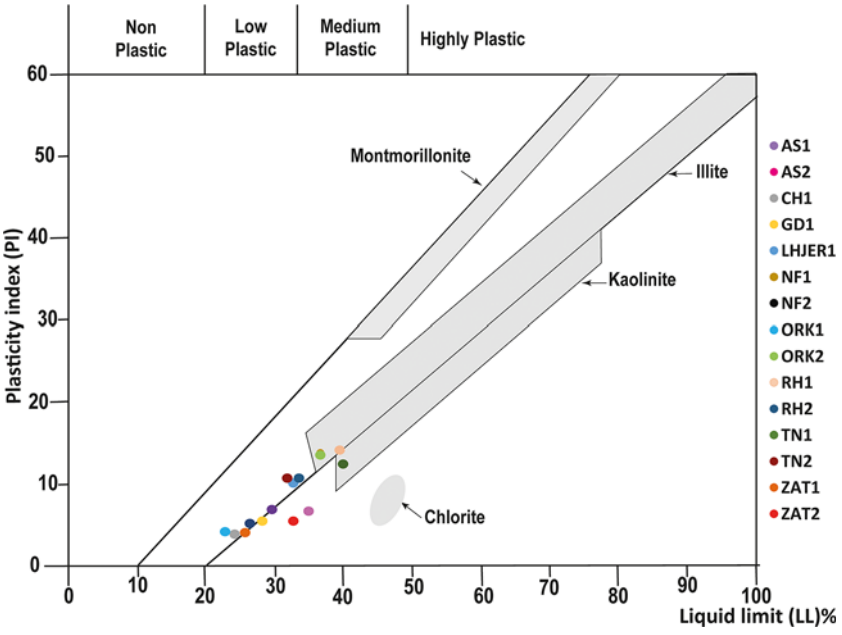

Figure 9. Projection of the studied clayey samples onto a diagram modified from Holtz & Kovacs (1981).

El Ouahabi *et al.*, 2019; Rahou *et al.*, 2022). A greater sand content increases porosity, leading to lower densification, compared to materials with a greater clay fraction (El Boudour El Idrissi *et al.*, 2018).

Based on the granulometric composition of the samples, the porosity and permeability were estimated using the McManus ternary diagram (Fig. 8b; McManus, 1988). Most samples exhibit moderate to high porosity and permeability due to their high silt and moderate sand contents. Given this context, increasing the clay fraction content is fundamental to making clay raw materials suitable for certain ceramic productions.

The PL values of the studied samples range from 18.5% to 28.1%, while the LL values range from 22.5% and 39.6% (Table 4). The PI of the samples varies between 3.7% and 13.9%. According to the diagram of Holtz & Kovacs (1981), most of the analysed clayey materials are classified as low-plasticity clays, except for samples AS2, NF1, ORK2, RH1, RH2 and TN1, which exhibit medium plasticity (Fig. 9).

The plasticity of clay materials is influenced by several factors, including their particle-size distribution, clay content and mineralogical composition (Boussen *et al.*, 2016; El Boudour El Idrissi *et al.*, 2016, 2021). Regarding the mineralogy of the clay fraction, illite, kaolinite and chlorite are associated with low plasticity, whereas smectite and fibrous clays are characterized by higher plasticity (Low, 1980; Sridharan & Choudhury, 2002; Daoudi *et al.*, 2015). The smectite content of the analysed samples is low, and fibrous clays are absent.

Plasticity variations are primarily attributed to the quantity and type of clay minerals. A higher proportion of clay minerals, particularly smectite and vermiculite, increases the plasticity. Accordingly, the most plastic samples (TN1, ORK2, RH1 and NF1) exhibit the greatest total clay content, along with a notable presence of these highly plastic minerals. Projection onto a PI–PL diagram (Bain & Highley, 1979) shows that they are not fully suitable for the ceramics industry (Fig. 10). Samples NF2, RH1, RH2, TN1, TN2 and ORK2 have PI values ≥10%, making them suitable for

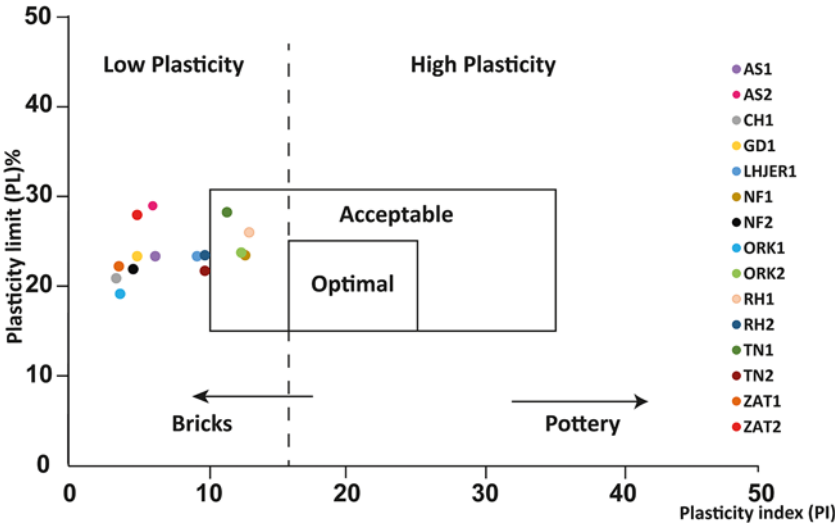

Figure 10. Projection of the studied clayey materials onto a diagram modified from Bain & Highley (1979).

industrial brick extrusion, whereas the other samples with lower PI values might crack during extrusion (de Souza Nandi *et al.*, 2023). All of the samples have too low plasticity for use in pottery; consequently, improvements in their plasticity are required to make them compatible with the requirements of this application.

The clayey sludges are chemically suitable for use in the ceramics industry. However, from a physical and mineralogical standpoint, certain modifications are necessary to optimize their properties, with the exception of sample TN1, which appears to be directly suitable for ceramics production. In this context, enhancing their characteristics requires the addition of clay fractions, particularly those with higher plasticity, such as smectite or fibrous clays. For instance, the mud from the reservoir of the Lalla Takerkoust Dam, which experienced high sedimentation rates, is rich in the clay fraction and is composed mostly of smectite (Gourfi *et al.*, 2023). The sediments of the Rocade Canal have similar characteristics (El Boudour El Idrissi *et al.*, 2018). These materials are suitable for blending with the studied sludges to create optimized formulations, thereby meeting the specific requirements for enhancing the overall ceramic performance. Furthermore, the heterogeneity of the investigated sludge samples provides an additional perspective regarding their valorization, including with regards to composites reinforced with natural fibres. Previous studies have shown that alfa fibres can improve the physicomechanical and thermal properties of construction materials (Garrouri *et al.*, 2022), and that natural fibres can reinforce ceramic slurry compacts (Avram *et al.*, 2024b), suggesting promising alternative applications of these materials.

Conclusion

Clayey sludges from aggregate washing in Marrakech quarries were valorized for their potential use in ceramic applications. Unlike other industrial sludges, which are often characterized by a uniform composition, the clayey sludges resulting from aggregate washing exhibited variability in terms of particle-size distribution, mineralogical composition and chemical properties. This variability was influenced by several factors, including the nature of the parent rock and the source location along the river. These sludges consist mainly of quartz, feldspars and clayey minerals. However, their low to medium plasticity, combined with their variable particle-size distribution, limited their direct valorization.

These clayey sludges could be used without additives for the production of red bricks. For other applications, such as pottery, specific formulations would be required involving blending the sludges with more plastic clays to modify their particle-size distribution and improve their plasticity to meet the requirements of these industrial processes.

The study highlights a dual benefit of using these clayey sludges, both environmental and economic. Firstly, doing so would reduce the discharge of waste materials through valorization. Secondly, doing so would provide a local alternative to clay materials being imported from other regions, thereby addressing the needs of regional ceramic producers for clay raw materials.

The clayey sludges from the Marrakech region represent an underexploited resource with significant potential for sustainable applications. However, further studies are essential to optimize these formulations and assess the performance of the finished products, ensuring their effective integration into targeted sectors. This approach could also serve as a model for other regions facing similar challenges, reinforcing efforts towards sustainable industrial waste management.

Supplementary material. The supplementary material for this article can be found at https://doi.org/10.1180/clm.2026.10027.

Acknowledgements. We thank Ayoub El Aallaoui for his significant support in the preparation of the figures. We also thank Mr Benoit Duchemin for performing the SEM imaging at the Laboratoire Ondes et Milieux Complexes, UMR 6294, CNRS – Université du Havre. Financial support was provided by the Project of National Center for Scientific and Technical Research (CNRST) 'Domaines Prioritaires de la Recherche Scientifique et du Développement Technologique/Ref. PPR1/2015/63'.

CRediT authorship contribution statement. Safaa Zahir: Conceptualization, Methodology, Data curation, Writing – original draft, Writing – review & editing. Lahcen Daoudi: Supervision, Conceptualization, Methodology, Writing – original draft, Writing – review & editing. Meriam El Ouahabi: Methodology, Writing – review & editing. Nathalie Fagel: Methodology, Writing – review & editing.

Competing interests. The authors declare none.

Data availability. The data that have been used are confidential.

References

AFNOR (1993) NF P 94-051 – Détermination des limites d'Atterberg limite de liquidité à la coupelle – Limite de plasticité au rouleau. Retrieved from https://www.boutique.afnor.org/fr-fr/norme/nf-p94051/sols-reconnaissance-et-essais-determination-des-limites-datterberg-limite-d/fa020765/11080.

AFNOR (1995) NF P94-052-1 -Détermination des limites d'Atterberg - Partie 1 : limite de liquidité - Méthode du cône de pénétration. Retrieved from https://www.boutique.afnor.org/fr-fr/norme/nf-p940521/sols-reconnaissance-et-essais-determination-des-limites-datterberg-partie-1/fa039276/11079.

April R.H., Hluchy M.M. & Newton R.M. (1986) The nature of vermiculite in Adirondack soils and till. *Clays & Clay Minerals*, **34**, 549–556.

Avram S.E., Birle B.V., Tudoran L.B., Borodi G. & Petean I. (2024a) Investigation of used water sediments from ceramic tile fabrication. *Water*, **16**, 1027.

Avram S.E., Tudoran L.B., Cuc S., Borodi G., Birle B.V. & Petean I. (2024b) Natural fiber reinforcement of ceramic slurry compacts. *Journal of Composite Science*, **8**, 542.

Avram S.E., Birle B.V., Cosma C., Tudoran L.B., Moldovan M., Cuc S. *et al.* (2025a) Ecological building material obtained through the moderate thermal consolidation of ceramic slurry collected from industrial waste waters. *Materials*, **18**, 1715.

Avram S.E., Tudoran L.B., Borodi G., Filip M.R. & Petean I. (2025b) Urban traffic's influence on noise and particulate matter pollution. *Sustainability*, **17**, 2077.

Aydinalp C. (2010) Some important properties and classification of Vertisols under Mediterranean climate. *African Journal of Agricultural Research*, **5**, 449–452.

Baccour H., Medhioub M., Jamoussi F. & Mhiri T. (2009) Influence of firing temperature on the ceramic properties of Triassic clays from Tunisia. *Journal of Materials Processing Technology*, **209**, 2812–2817.

Bain J.A. & Highley D.E. (1979) Regional appraisal of clay resources – a challenge to the clay mineralogist. Pp. 437–446 in: *Developments in Sedimentology* (M.M. Mortland & V.C. Farmer, editors). Elsevier, London, UK.

Bennour A., Mahmoudi S., Srasra E., Hatira N., Boussen S., Ouaja M. & Zargouni F. (2015) Identification and traditional ceramic application of clays from the Chouamekh region in south-eastern Tunisia. *Applied Clay Science*, **118**, 212–220.

Boski T., Pessoa J., Pedro P., Thorez J., Dias J.M.A. & Hall I.R. (1998) Factors governing abundance of hydrolyzable amino acids in the sediments from the N.W. European Continental Margin (47–50°N). *Progress in Oceanography*, **42**, 145–164.

Boussen S., Sghaier D., Chaabani F., Jamoussi B. & Bennour A. (2016) Characteristics and industrial application of the Lower Cretaceous clay deposits (Bouhedma Formation), southeast Tunisia: potential use for the manufacturing of ceramic tiles and bricks. *Applied Clay Science*, **123**, 210–221.

Carretero M.I., Dondi M., Fabbri B. & Raimondo M. (2002) The influence of shaping and firing technology on ceramic properties of calcareous and non-calcareous illitic-chloritic clays. *Applied Clay Science*, **20**, 301–306.

Castellanos H.G., Aryanfar Y., Keçebaş A., Assad M.E.H., Islam S., Naveed Q.N. & Lasisi A. (2024) A new paradigm for mining energy from industrial sludge: a low-cost fuel. *Journal of Water Process Engineering*, **59**, 2214–7144.

Cook H.E., Johnson P.D., Matti J.C. & Zemmels I. (1975) Methods of sample preparation and X-ray difraction data analysis. Institute of Geophysic and Planetary Physics. Retrieved from https://deepseadrilling.org/28/volume/dsdp28_appendixIV.pdf.

Daoudi L., Hicham E.E., Latifa S., Abderrahmane A., Jamal B., Mohamed W. *et al.* (2014) Characteristics and ceramic properties of clayey materials from Amezmiz region (western High Atlas, Morocco). *Applied Clay Science*, **102**, 139–147.

Daoudi L., Knidiri A., El Boudour El Idrissi H., Rhouta B. & Fagel N. (2015) Role of the texture of fibrous clay minerals in the plasticity behavior of host materials (Plateau du Kik, western High Atlas, Morocco). *Applied Clay Science*, **118**, 283–289.

de Souza Nandi V., Zaccaron A., Raupp-Pereira F., Arcaro S., Bernardin A.M. & Montedo O.R.K. (2023) Plastic behaviour of clay materials for the manufacture of fast-drying red ceramics. *Clay Minerals*, **58**, 26–37.

Dondi M., Raimondo M. & Zanelli C. (2014) Clays and bodies for ceramic tiles: reappraisal and technological classification. *Applied Clay Science*, **96**, 91–109.

El Aallaoui A., Elghali A., Hakkou R., Taha Y., Benzaazoua M. & El Ghorfi M. (2025) 3D geometallurgical characterization of coal mine waste rock piles for their reprocessing purpose. *International Journal of Coal Science and Technology*, **12**, 16.

El Boudour El Idrissi H., Daoudi L., El Ouahabi M., Balo Madi A., Collin F. & Fagel N. (2016) Suitability of soils and river deposits from Marrakech for the manufacturing of earthenware. *Applied Clay Science*, **129**, 108–115.

El Boudour El Idrissi H., Daoudi L., El Ouahabi M., Collin F. & Fagel N. (2018) The influence of clay composition and lithology on the industrial potential of earthenware. *Construction and Building Materials*, **172**, 650–659.

El Boudour El Idrissi H., Borja W., Fagel N. & Daoudi L. (2021) Simple approach to elaborate test bricks for traditional ceramic studies. *Engineering Archive engrxiv*. Retrieved from https://doi.org/10.31224/osf.io/4b37g.

El Khalki E.M., Tramblay Y., Amengual A., Homar V., Romero R., Saidi M.E.M. & Alaou M. (2020) Validation of the AROME, ALADIN and WRF meteorological models for flood forecasting in Morocco. *Water*, **12**, 437.

El Ouahabi M., Daoudi L., Hatert F. & Fagel N. (2015) Modified mineral phases during clay ceramic firing. *Clays and Clay Minerals*, **63**, 404–413.

El Ouahabi M., El Boudour El Idrissi H., Daoudi L., El Halim M. & Fagel N. (2019) Moroccan clay deposits: physico-chemical properties in view of provenance studies on ancient ceramics. *Applied Clay Science*, **172**, 65–74.

Fatah T.A., Zhang R., Huang X., Zheng J., Miao Y. & Mastoi A.K. (2021) Strength and leaching behavior of contaminated mining sludge at high water content stabilized with lime activated GGBS. *Materials*, **14**, 6524.

Ferrari S. & Gualtieri A.F. (2006) The use of illitic clays in the production of stoneware tile ceramics. *Applied Clay Science*, **32**, 73–81.

Fiori C., Fabbri B., Donati G. & Venturi I. (1989) Mineralogical composition of the clay bodies used in the Italian tile industry. *Applied Clay Science*, **4**, 461–473.

Galetakis M., Alevizos G. & Leventakis K. (2012) Evaluation of fine limestone quarry by-products, for the production of building elements – an experimental approach. *Construction and Building Materials*, **26**, 122–130.

Garrouri S., Lakhal W., Benazzouk A. & Sediki E. (2022) Potential use of alfa fibers in construction material: physico-mechanical and thermal characterisation of reinforced specimen. *Construction and Building Materials*, **342**, 127787.

Garzón E., Sánchez-Soto P.J. & Romero E. (2010) Physical and geotechnical properties of clay phyllites. *Applied Clay Science*, **48**, 307–318.

González-Corrochano B., Alonso-Azcárate J. & Rodas M. (2009) Characterization of lightweight aggregates manufactured from washing aggregate sludge and fly ash. *Resources, Conservation and Recycling*, **53**, 571–581.

Gourfi A., Daoudi L., Rhoujjati A., Benkaddour A. & Fagel N. (2020) Use of bathymetry and clay mineralogy of reservoir sediment to reconstruct the recent changes in sediment yields from a mountain catchment in the western High Atlas region, Morocco. *Catena*, **191**, 104560.

Gourfi A., Daoudi L., Ben Daoud N. & Fagel N. (2023) Clay minerals in soils and sediment as tracers of provenance: the case study of the N'fis watershed, Morocco. *Soil Use and Management*, **40**, 1–20.

Gugliotta M., Saito Y., Ta T.K.O., Nguyen V.L., Uehara K., Tamura T. *et al.* (2020) Sediment distribution along the fluvial to marine transition zone of the Dong Nai River System, southern Vietnam. *Marine Geology*, **429**, 106314.

Haida S., Snoussi M., Latouche C. & Probst J.L. (1996) Géodynamique actuelle du bassin versant de l'Oued Tensift (Maroc) : érosion mécanique et bilan des transports solides fluviaux./Present geodynamic of the Tensift drainage basin (Morocco): mechanical erosion and fluvial transports of sediments. *Sciences Géologiques. Bulletin*, **49**, 7–23.

Hajhouji Y. (2018) *Modélisation hydrologique du bassin versant de l'oued Rheraya et sa contribution à la recharge de la nappe du Haouz (bassin du Tensift, Maroc)*. Thesis. Université de Toulouse.

Haut Commissariat au Plan (2020) *Monographie Regionale Region de Marrakech – Safi Annee 2018*. Haut Commissariat au Plan, Paris, France, 125 pp.

Heiri O., Lotter A. & Lemcke G. (2001) Loss on ignition as a method for estimating organic and carbonate content in sediments. *Journal of Paleolimnology*, **25**, 101–110.

Holtz R.D. & Kovacs W.D. (1981) *An Introduction to Geotechnical Engineering*, 1st edition. Prentice-Hall, Englewood Cliffs, NJ, USA, 733 pp.

Holtzapffel T. (1985) Les mineraux argileux. Préparation. Analyse diffractométrique et détermination. *Annales de la Société géologique du Nord*, **12**, 15–43.

Khalfaoui A. & Hajjaji M. (2009) A chloritic-illitic clay from Morocco: temperature–time–transformation and neoformation. *Applied Clay Science*, **45**, 83–89.

Kłosek-Wawrzyn E., Łój G., Bugaj A. & Wons W. (2019) Waste sludge from washing dolomite aggregates as a raw material for brick production. *Gospodarka Surowcami Mineralnymi – Mineral Resources Management*, **35**, 37–48.

Knidiri A., Daoudi L., El Ouahabi M., Rhouta B., Rocha F. & Fagel N. (2014) Palaeogeographic controls on palygorskite occurrence in Maastrichtian–Palaeogene sediments of the western High Atlas and Meseta basins (Morocco). *Clay Minerals*, **49**, 595–608.

Kologrieva U., Volkov A., Krasnyanskaya I., Stulov P. & Wainstein D. (2022) Analysis of hydrometallurgical methods for obtaining vanadium concentrates from the waste by chemical production of vanadium pentoxide. *Materials*, **15**, 938.

Kreimeyer R. (1987) Some notes on the firing colour of clay bricks. *Applied Clay Science*, **2**, 175–183.

Laita E. & Bauluz B. (2018) Mineral and textural transformations in aluminium-rich clays during ceramic firing. *Applied Clay Science*, **152**, 284–294.

Lee V.G. & Yeh T.H. (2008) Sintering effects on the development of mechanical properties of fired clay ceramics. *Materials Science and Engineering: A*, **485**, 5–13.

Loutou M., Hakkou R., Argane R., Mansori M., Grase L., Svinka R. & Mezinskis G. (2018) Clayey quarry sludges: thermal transformation, microstructure and technological properties. *Waste and Biomass Valorization*, **9**, 1805–1815.

Low P.F. (1980) The swelling of clay: II. Montmorillonites 1. *Soil Science Society of America Journal*, **44**, 667–676.

Luo C., Deng Y., Inubushi K., Liang J., Zhu S., Wei Z. *et al.* (2018) Sludge biochar amendment and alfalfa revegetation improve soil physicochemical properties and increase diversity of soil microbes in soils from a rare earth element mining wasteland. *International Journal of Environmental Research and Public Health*, **15**, 965.

Maalla I., Boussen S., Fagel N. & Mohamed Essghaier G. (2021) Incorporation of siliceous sand and lignite tailings from Miocene deposits (Zeramdine, eastern Tunisia) in clay bricks and ceramic tiles: technological feasibility. *Arabian Journal of Geosciences*, **14**, 282.

Madejova J. (2003) FTIR techniques in clay mineral studies. *Vibrational Spectroscopy*, **31**, 1–10.

Magalhães C.P., Alves J.I., Duber A., Oleskowicz-Popiel P., Stams A.J.M. & Cavaleiro A.J. (2024) Metabolic versatility of anaerobic sludge towards platform chemical production from waste glycerol. *Applied Microbiology and Biotechnology*, **108**, 419.

Maletsika P.A., Nanos G.D. & Stavroulakis G.G. (2015) Peach leaf responses to soil and cement dust pollution. *Environmental Science and Pollution Research*, **22**, 15952–15960.

Martínez-García C., Eliche-Quesada D., Pérez-Villarejo L., Iglesias-Godino F.J. & Corpas-Iglesias F.A. (2012) Sludge valorization from wastewater treatment plant to its application on the ceramic industry. *Journal of Environmental Management*, **95**, S343–S348.

Maston O., Ouahbi T., Taibi S., El-Hajjar A., Sapin L., Esnault-Filet A. *et al.* (2025) Effect of MICP treatment on the mechanical properties of clay soils. *Transportation Geotechnics*, **50**, 101483.

McManus J. (1988) Grain size distribution and interpretation. Pp. 63–85 in: *Techniques in Sedimentology* (M.E. Tucker, editor). Blackwell Scientific Publications, Oxford, UK.

Mercantili L., Davis F. & Higson S.P.J. (2013) Ultrasonic initiation of the alkaline hydrolysis of triglycerides (saponification) without phase catalysis. *Journal of Surfactants and Detergents*, **16**, 337–344.

Michard A., Saddiqi O., Chalouan A. & Frizon de Lamotte D. (editors) (2008) *Continental Evolution: The Geology of Morocco: Structure, Stratigraphy, and Tectonics of the Africa–Atlantic–Mediterranean Triple Junction*. Lecture Notes in Earth Sciences 116. Springer, Dordrecht, The Netherlands, 444 pp.

Miliani P. & Corbara F. (1999) *Tecnologia, Ceramica – Le Materie Prime*. Gruppo Editoriale Faenza Editrice, Faenza, Italy, 97 pp.

Ministère de l'Equipement du Transport et de la Logistique (2016) *Grands chantiers et réformes 2012–2016*. Ministère de l'Equipement du Transport et de la Logistique, Rabat, Morocco, 141 pp.

Ministère de l'Équipement et du Transport (2012) *Inventaire des carrières*. Ministère de l'Équipement et du Transport, Rabat, Morocco, 165 pp.

Moore D.M. & Reynolds J.R. (1997) *X-Ray Diffraction and the Identification and Analysis of Clay Minerals*. Oxford University Press, New York, NY, USA, 378 pp.

Murray H.H. (2007) *Applied Clay Mineralogy: Occurrences, Processing and Applications of Kaolins, Bentonites, Palygorskitesepiolite, and Common Clays*. Elsevier, Amsterdam, The Netherlands, 473 pp.

Rahou J., Rezqi H., El Ouahabi M. & Fagel N. (2022) Characterization of Moroccan steel slag waste: the potential green resource for ceramic production. *Construction and Building Materials*, **314**, 125663.

Sadek H.E.H., Hessien M.A., Abd El-Shakour Z.A., Taha M.A. & Khattab R.M. (2021) The effect of sintering on the properties of magnesia–granite sludge ceramics shaped by temperature-induced forming. *Journal of Materials Research and Technology*, **11**, 264–273.

Saidi M.E., Daoudi L., Aresmouk M.E.H. & Blali A. (2003) Rôle du milieu physique dans l'amplification des crues en milieu montagnard : exemple de la crue du 17 août 1995 dans la vallée de l'Ourika (Haut-Atlas, Maroc). *Secheresse*, **14**, 107–114.

Saikia N.J., Bharali D.J., Sengupta P., Bordoloi D., Goswamee R.L., Saikia P.C. & Borthakur P.C. (2003) Characterization, beneficiation and utilization of a kaolinite clay from Assam, India. *Applied Clay Science*, **24**, 93–103.

Shepard F.P. (1954) Nomenclature based on sand-silt-clay ratios. *Journal of Sedimentary Petrology*, **14**, 256–259.

Sridharan A. & Choudhury D. (2002) Swelling pressure of sodium montmorillonites. *Geotechnique*, **52**, 459–462.

Strazzera B., Dondi M. & Marsigli M. (1997) Composition and ceramic properties of Tertiary clays from southern Sardinia (Italy). *Applied Clay Science*, **12**, 247–266.

Tarte P. (1967) Infra-red spectra of inorganic aluminates and characteristic vibrational frequencies of AlO tetrahedra and AlOs octahedra. *Spectrochimica Acta Part A: Molecular Spectroscopy*, **23**, 2127–2143.

Thorez J. (1976) *Practical Identification of Clay Minerals*. G. Lelotte, Dison, Belgium 90 pp.

Tomanec R., Popov S., Vučinič D. & Lazič P. (1997) Vermiculite From Kopaonik (Yugoslavia) characterization and processing. *Fizykochemiczne Problemy Mineralurgii*, **31**, 247–254.

Trindade M.J., Dias M.I., Coroado J. & Rocha F. (2009) Mineralogical transformations of calcareous rich clays with firing: a comparative study between calcite and dolomite rich clays from Algarve, Portugal. *Applied Clay Science*, **42**, 345–355.

Trindade M.J., Dias M.I., Coroado J. & Rocha F. (2010) Firing tests on clay-rich raw materials from the Algarve Basin (southern Portugal): study of mineral transformations with temperature. *Clays and Clay Minerals*, **58**, 188–204.

Unuabonah E.I., Gu C., Weber J., Lubahn S. & Taubert A. (2013) Hybrid clay: a new highly efficient adsorbent for water treatment. *ACS Sustainable Chemistry & Engineering*, **1**, 966–973.

Vashistha P., Kumar V., Singh S.K., Dutt D., Tomar G. & Yadav P. (2019) Valorization of paper mill lime sludge *via* application in building construction materials: a review. *Construction and Building Materials*, **211**, 371–382.

Veerasingam S. & Venkatachalapathy R. (2014) Estimation of carbonate concentration and characterization of marine sediments by Fourier

transform infrared spectroscopy. *Infrared Physics & Technology*, **66**, 136–140.

Wang S., Pan C., Xie D., Xu M., Yan Y. & Li X. (2022) Grain size characteristics of surface sediment and its response to the dynamic sedimentary environment in Qiantang Estuary, China. *International Journal of Sediment Research*, **37**, 457–468.

Zajec L., Gradinjan D., Klančnik K. & Gaberščik A. (2016) Limestone dust alters the optical properties and traits of *Fagus sylvatica* leaves. *Trees – Structure and Function*, **30**, 2143–2152.

Zia-Khan S., Spreer W., Pengnian Y., Zhao X., Othmanli H., He X. & Müller J. (2015) Effect of dust deposition on stomatal conductance and leaf temperature of cotton in northwest China. *Water*, **7**, 116–131.